Journal of Computer-Aided Molecular Design, **12:** 147–163, 1998.
KLUWER/ESCOM

Structural models of antibody variable fragments: A method for investigating binding mechanisms

Samuel Petit[a,*], Frédéric Brard[b,**], Gérard Coquerel[a,***], Guy Perez[a] & François Tron[b]
[a]*Laboratoire de Modélisation Moléculaire, IRCOF, IFRMP No. 23, Université de Rouen, Rue Tesnières, F-76821 Mont-Saint-Aignan Cedex, France*
[b]*Groupe de Recherche en ImmunoPathologie, IFRMP No. 23, UFR de Médecine-Pharmacie, CHU de Rouen, F-76031 Rouen Cedex, France*

Received 29 January 1997; Accepted 15 September 1997

Key words: anti-(H2A-H2B) autoantibodies, antigen binding mechanism, comparative molecular modeling, electrostatic interactions, nucleosome, systemic lupus erythematosus

Summary

The value of comparative molecular modeling for elucidating structure–function relationships was demonstrated by analyzing six anti-nucleosome autoantibody variable fragments. Structural models were built using the automated procedure developed in the COMPOSER software, subsequently minimized with the AMBER force field, and validated according to several standard geometric and chemical criteria. Canonical class assignment from Chothia and Lesk's [Chottin and Lesk, J. Mol. Biol., 196 (1987) 901; Chothia et al., Nature, 342 (1989) 877] work was used as a supplementary validation tool for five of the six hypervariable loops. The analysis, based on the hypothesis that antigen binding could occur through electrostatic interactions, reveals a diversity of possible binding mechanisms of anti-nucleosome or anti-histone antibodies to their cognate antigen. These results lead us to postulate that anti-nucleosome autoantibodies could have different origins. Since both anti-DNA and anti-nucleosome autoantibodies are produced during the course of systemic lupus erythematosus, a non-organ specific autoimmune disease, a comparative structural and electrostatic analysis of the two populations of autoantibodies may constitute a way to elucidate their origin and the role of the antigen in tolerance breakdown. The present study illustrates some interests, advantages and limits of a methodology based on the use of comparative modeling and analysis of molecular surface properties.

Introduction

As one of the main goals of structural biology, the understanding of structure–function relationships has led to the development of numerous promising research projects, which involve the collaborative efforts of biologists, chemists and physicists. To date, X-ray diffraction or NMR techniques have been the most valuable tools for elucidating structure–function relationships of biological molecules [1–3]. Although the application of these experimental methods is continually growing, they remain time-consuming and of limited applicability due to difficulties with crystallization and/or insufficient quantities of accurate experimental data [4,5]. In connection with the increasing number of resolved protein structures [6], several modeling methods have appeared during the last few years [7,8] which aim at predicting tertiary structures. Two distinct strategies have emerged from these works, namely energy-based and knowledge-based methods [9–11]. Algorithms combining both methods have also been developed [12].

Molecules in the immunoglobulin (Ig) superfamily contain one or more domains known as Ig fold. Each Ig fold contains a disulfide bridge and approximately 100 amino acids [13]. The highly conserved folding of

*Present address: Novartis Pharma AG, S.360.10.20, CH-4002 Basel, Switzerland. **Present address: Department of Molecular Biology, Princeton University, Princeton, NJ 08544, U.S.A. *** To whom correspondence should be addressed.

this protein family and the quantity of experimentally determined 3D structures of Ig make this superfamily ideal for modeling using a knowledge-based strategy. In order to understand the antigen binding mechanism of a specific antibody (Ab), it is necessary to determine the 3D structure of its variable fragment (Fv) since antigen–Ab interactions usually involve a restricted area of this fragment, the so-called Ab combining site [14–17]. The Fv fragment is a non-covalent association of two variable domains belonging to the heavy (VH) and light (VL) chains (about 120 and 110 residues, respectively). The residues most frequently involved in antigen binding are essentially located in six regions termed the complementarity-determining regions (CDRs), first defined by Kabat et al. [18] as regions of high variability in nucleic acid sequences. Three CDRs (H1, H2, H3) are located on VH and three others (L1, L2, L3) on VL. The highest variability is observed for the third CDR of the heavy chain, CDR-H3.

At the 3D level, Chothia, Lesk et al. [19,20] have defined six Fv hypervariable (HV) loops with positions and lengths close but not identical to those of the CDRs. For five of the HV loops, the number of canonical conformations, arising from the presence of a few key residues, is limited. Canonical class assignments allow a prediction of the conformations for these five HV loops.

AutoAbs (i.e., Abs directed against self-antigens) reacting with the (H2A-H2B) histone dimer are produced by mice which spontaneously develop an autoimmune disease similar to the human systemic lupus erythematosus (SLE) [21]. The origin of these autoAbs is unknown. The (H2A-H2B) dimer is a constituent part of a physiological nucleoproteic complex, the nucleosome (Figure 1), which is composed of a histone octamer ($(H2A\text{-}H2B)_2$ and $(H3\text{-}H4)_2$) associated with two loops of double-stranded DNA (dsDNA) linked by an H1 histone molecule [22]. Numerous data have led to the supposition that anti-(H2A-H2B) autoAbs could be pathogenic [23], and murine models of SLE are extensively used in attempts to understand anti-histone Ab origin and physiopathologic mechanisms [24]. Structure–origin relationship investigations of Abs are facilitated by the fact that antigen-driven responses result in the expression of structural stigmas such as particular amino acids on Ab combining sites.

The present paper reports the construction and analysis of Fv 3D structural models of six anti-(H2A-H2B) monoclonal antibodies (mAbs) by comparative modeling. We have previously shown [25] that anti-(H2A-H2B) and anti-DNA Abs share common primary structural features and similar mutation patterns. These results led us to propose that the nucleosome could be the anionic/cationic autoantigen that elicits anti-DNA and anti-(H2A-H2B) Ab production and to envisage a filial relationship between these two Ab populations. According to several authors [26,27], ionic interactions are involved in antigen binding of anti-DNA Abs, which is consistent with the polyanionic character of DNA. We have therefore formulated the hypothesis that the specificity of anti-(H2A-H2B) and anti-nucleosome Abs could also be mainly due to ionic attraction. This would be consistent, on the one hand, with the high frequency of charged residues in the CDRs of anti-(H2A-H2B) Abs [25] and, on the other hand, with the presence of numerous cationic residues in histone terminal domains. Our analysis of ionic binding potentialities was completed with model analysis to look for the possible involvement of other types of interactions such as cation-π interactions [28].

Materials and methods

Selection of anti-(H2A-H2B) mAb Fv

Anti-(H2A-H2B) mAb primary sequences have been obtained from our previous work [25], from the literature [29,30] or from nucleotide databases (GenBank/EMBL/DDBJ). Table 1 summarizes the references and accession numbers of the six selected mAbs. All these Abs are derived from different lupus prone mice and use various genetic characteristics and isotypes. They were selected for their common fine specificity.

Building principles and elaboration of an Ig structural database

The multiple modeling methods devoted to the construction of protein structural models have been recently reviewed by Vasquez et al. [31]. While many models are still constructed at least in part by manual methods on graphic devices, automated procedures have come into greater use. Initially developed by Blundell's group [32], COMPOSER is one of the first pieces of software using a multiple-structure approach and an automated procedure for comparative modeling of protein tertiary structures [33]. Interfaced with SYBYL software [34], COMPOSER operates easily

Table 1. Identity, accession numbers and bibliographic references of the six selected anti-(H2A-H2B) mAbs

Antibody	Isotype	VH Ac.nb.[a]	VL Ac.nb.[a]	Reference
3F6	IgG2a, κ	Z37145	Z50032	25
2E1	IgG2a, κ	Z66551	Z66552	25
13D10	IgG2a, κ	U51463	U51464	–[b]
LG4-3	IgG2b, λ	X65004	X65012	30
B/SB5-28	IgG2b, κ	NS[c]	NS[c]	29
6E5	IgG2b, λ	U51458	U51460	–[b]

– [a]Ac.nb. stands for accession numbers in GenBank/EMBL/DDBJ library.
– [b]F. Jovelin, H. Chabre, Z. Amoura, D. Gilbert, J.F. Bach and S. Koutouzov, manuscript in preparation.
– [c]NS stands for Non Submitted.

and rapidly on 3D workstations. The present study was achieved with the 6.2 version (1995) of SYBYL implemented on a 4D-210 GTX Silicon Graphics workstation (Power Series).

The COMPOSER methodology is based on two principles deduced from protein crystal structure analyses. The more general principle arises from a study which showed that functionally and sequentially related proteins have a common tertiary folding pattern [35,36]. This implies that primary sequence homologies should give valuable data for building a structural model from a set of homologs. The second principle distinguishes between two types of structural regions in a given family of proteins: on the one hand, the structurally conserved regions (SCRs) define the global architecture of the molecules and are almost identical for all the molecules of the family; on the other hand, the structurally variable regions (SVRs or loops) are fragments of shorter length which link together the successive SCRs and correspond to the structural differences between the members of the family.

The use of COMPOSER requires two types of data: the primary sequence of the protein or fragment to be modeled and a database containing the structural information for a number of crystallized related proteins. Since our work deals with a protein family (immunoglobulins) of great structural homogeneity and conservation, we decided to build our own database of immunoglobulins rather than use the more diversified one supplied with COMPOSER. The 155 crystal structures of our database were extracted from the Brookhaven Protein Databank (PDB) [37] via an ftp server (PDB releases of 1995). This large number of experimentally resolved structures is highly favorable for the use of a knowledge-based procedure. However, among the 155 structures, about 50% are very closely related or derived from one another.

Building procedure of structural models

The building procedure requires several steps. In the first step, the amino acid sequence of the unknown structure is systematically compared with those of the structural database using the alignment method of Needleman and Wunsch [38]. For each aligned sequence pair, the percentage of residue positions having the same amino acid in both sequences is calculated on the basis of a homology matrix. In this work, we used the matrix *swiss2* computed by Gonnet et al. [39]. The overall identity scores obtained for Fv heavy and light chains varied from 65% to 90% which corresponds to highly satisfactory scores: it is usually admitted that the minimum acceptable identity score is about 35% [32]. Among the 155 structures of our database, only the 142 with a resolution less than 3.0 Å were used for this homolog identification step. Furthermore, when two or more closely related homologs were identified, only one representative was conserved for the following steps. The list of the Igs used as structural templates is presented in Table 3.

Starting with a selection of the few best homologs, the second step of the COMPOSER procedure consists of generating a 3D structural alignment for the group of homologs (Figure 2a). Only C^{α} coordinates are considered in this step. The optimal structural alignment is obtained by performing a series of pairwise weighted least-square fits until convergence and is used to determine the SCRs. The regions of at least three residues for which no residue departs significantly (3 Å) from the mean corresponding position are

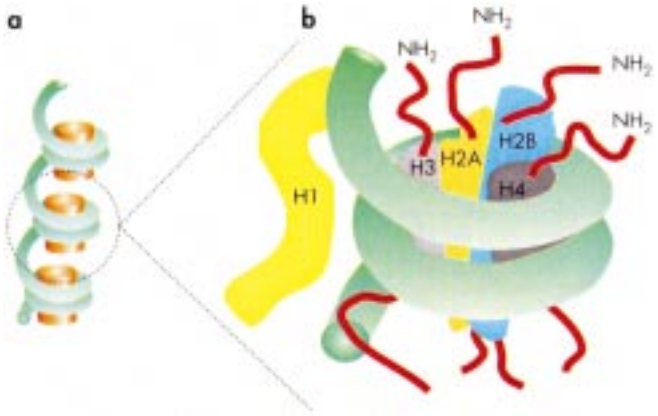

Figure 1. Schematic representation of the nucleosome structure. (a) The chromatin is composed of repeated elementary units named nucleosomes. (b) The nucleosome is formed by the association of a proteic moiety (histones H2A, H2B, H3, H4) organized as an octamer surrounded with a double-stranded DNA fragment of about 200 base pairs. The H1 histone is located at the surface of this structure in order to fix the DNA loop.

defined as SCRs. SVRs (loops) are the fragments for which this condition is not satisfied.

The third step is the construction of the model protein SCRs from the corresponding fragments of the homologous proteins. Each SCR of the model is built by selecting the best homolog for this SCR and by fitting the corresponding fragment in order to deduce atomic coordinates. Where there are different side chains between model and homolog, a standard library conformation is selected.

The last step of the COMPOSER procedure is the construction of the missing parts of the molecule, i.e., the loops. Both geometric information and sequence information are used to select a compatible fragment. The geometric criteria calculate the root mean square (rms) distance for the six anchor C^{α} atoms (three on each side of the loop). Among the possible loops, the best choice corresponds to a compromise between a low value of rms distance and a high identity score. In general, long loops are less likely to be correctly modeled than short ones. When an SVR corresponds to an HV loop as defined by Chothia and Lesk [19,20], the choice of a template fragment can be improved by choosing loops issued from a structure containing identical key residues.

In the particular case of B/SB5-28 Ab, residues 1–8 of the heavy chain primary sequence published by Portanova et al. [29] are missing. In order to complete the model, we have selected the corresponding sequence from a highly homologous Ab and built the 1–8 fragment as a supplementary loop of the molecule, using W3129 Ab (PDB code: 1FVW) as the fragment template (88% of identity).

Construction procedure for the CDR-H3 loops

Due to its high variability in terms of length and amino acid sequence, the CDR-H3 is often associated with a long SVR, as shown in Figure 2b. The largest potential source of error in the whole building procedure comes from the construction of this SVR because of the difficulty in finding suitable templates. Since the usual criteria, based on sequence identities and rms distances for anchor atom regions, were insufficient for a satisfactory construction of these SVRs, we developed a series of supplementary criteria from which a template fragment could be selected as the best compromise. The procedure we used is as follows. First, the construction of the SVR corresponding to CDR-H3 was based on consideration of all other loops of the Fv model. This allowed visualization of the steric environment of the CDR-H3 loop (including the light chain), and elimination of incorrect van der Waals contacts for certain of the possible fragments. Among the possible templates, we favored candidates issued from other CDRs rather than fragments belonging to framework regions. When only a small number of candidates were available from our Ig database, we extended our research using the more diversified SYBYL database. Finally, after a preliminary selection, we based our definitive choice on a visual analysis of the binding site conformation obtained, taking into account structural observations from other Fv crystal structures.

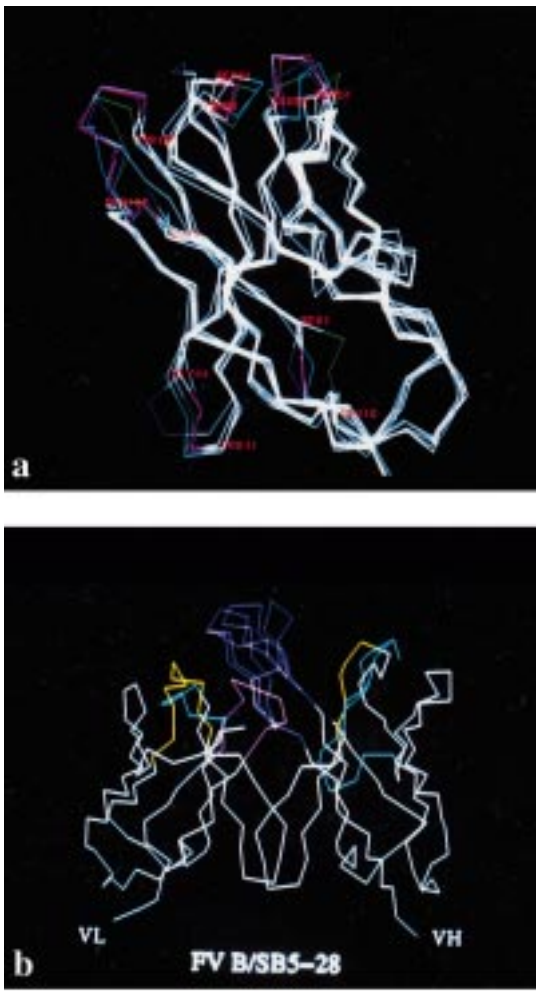

Figure 2. Superimposition of structural templates for 3D building of Fv models using the COMPOSER software. (a) Superimposition of the six templates used for the heavy chain of Fv 3F6. SCRs are in white and SVRs are colored. (b) Superimposition of three possible loop templates corresponding to the H3 loop of B/SB5-28.

Minimization and association of heavy and light chains

Once the final model structure is obtained, refinement and validation of the structure are necessary. The refinement procedure used was composed of three steps. First, we undertook manual corrections of the strongest incorrect van der Waals contacts by means of local and limited geometric modifications. Then, an energy minimization restricted to side-chain atoms was achieved and, finally, the minimization was extended to the whole model. The standard SYBYL minimizer (Powell method [40]) and the all-atom AMBER force field [41,42] were used. Electrostatic energy terms were computed using partial atomic charges loaded from the Kollman dictionary [43]. A distance-dependent dielectric function was chosen in order to correct for overestimation of intramolecular electrostatic interactions.

Because heavy and light variable domains of each Fv fragment (except the CDR-H3 loop) were constructed separately with COMPOSER, we had to dock the two minimized and validated chains. This was achieved by means of a superimposition of each modeled V-region on the crystal structure of a well-studied Fv. For antibodies with κ light chain, McPC603 (PDB code: 1MCP) was chosen as a template for superimposition, while Hc19 (PDB code: 1GIG) was used for λ light chains. The superimposition procedure consisted in selecting all the fragments of at least three residues located outside the hypervariable regions and for which both the reference sequence and the studied sequence were identical. Depending on framework identities, between 50 and 80 residues were therefore considered, and only backbone atoms were used for fitting. Root mean square deviations, computed for the fitted atoms, varied between 0.1 Å and 0.9 Å. Only minor geometric corrections or localized minimizations were necessary to obtain a satisfactory Fv structural model.

Validation of the final models

The validation of the model was achieved using the PROCHECK 3.2 software [44]. PROCHECK produces Ramachandran diagrams (statistical analysis of φ-ψ angle distribution) and also allows the examination of many structural features such as backbone and side-chain conformations (bond lengths and angles), secondary structures and exposure of residues to the solvent.

Another important aspect of the validation step consisted of comparing the conformations obtained for five of the six hypervariable regions (H1, H2, L1, L2 and L3) with those predicted from the Chothia and Lesk analyses of primary sequences [19,20,45]. Our structural models were superimposed with reference Fv crystal structures (Table 2). No significant conformational differences were observed.

Computation of electrostatic potentials on Fv molecular surfaces

The MOLCAD software [46], interfaced with SYBYL 6.2, was used to compute electrostatic potentials on molecular surfaces. For each Fv structure of interest,

Table 2. Position and length of hypervariable loops according to Chothia and Lesk [19,20][a] and canonical class assignment for five of the six HV loops[b]; for comparative purposes, positions of Kabat CDRs are given

HV regions	Kabat CDRs	Chothia and Lesk	3F6	2E1	13D10	LG4-3	B/SB5-28	6E5
L1	24–34 (13 res.)	26–32 (9 res.)	2 (HyHEL-10)	2	2	7 (Hc19)	2	7
L2	50–56 (7 res.)	50-52 (3 res.)	1 (J539)	1	1	1	1	1
L3	89–97 (9 res.)	91-96 (6 res.)	1 (McPC603)	1	1	4 (Hc19)	1	4
H1	31–35 (5 res.)	26–32 (7 res.)	1 (J539)	1	1	1	1	1
H2	50–65 (17 res.)	52A-55 (4 res.)	2 (8F5)	2	4 (McPC603)	2	3 (J539)	1 (Hc19)
H3	95–102 (11 res.)	96-101 (9 res.)	/	/	/	/	/	/

[a] Mean lengths of CDRs and HV loops are indicated in brackets.
[b] Martin numbering [45], which completes that of Chothia and Lesk, is used. The name of a representative member is given for each class. PDB codes of these reference structures are HyHEL-10: 3HFM; Hc19: 1GIG; J539: 2FBJ; McPC603: 1MCP; 8F5: 1BBD.

an isosurface of electron densities similar to surfaces generated with Connolly's MS program [47] was calculated, with a factor 1.5 applied to van der Waals radii. On each grid point of the obtained surface, the density represents the sum of all atom densities contributing to this sample point. The molecular electrostatic potential (EP) was computed on each point (i) of the electron density surfaces using Kollman atomic charges (q_j) and a Coulombic-type equation:

$$EP(i) = \sum_{j=1}^{N} \frac{q_j}{r_{ij}}$$

where r_{ij} is the distance between point i and atom j.

Selection of irrelevant antibodies

Since our purpose is to identify common features shared by anti-(H2A-H2B) Abs from their 3D Fv structure, we have selected (Table 3) a group of 13 Abs for which the crystal structure of the Fv has been determined by X-ray diffraction techniques and is available in the Brookhaven PDB. The selection was carried out as follows. We first established a list of the homologs of murine origin and selected as possible templates by COMPOSER for the construction of large SCRs (more than 20 residues). Then we listed the specificities of these Abs, and when several had the same specificity, we retained only the one with the lowest resolution factor. The only exception is Hc19, which has been chosen as a representative of Abs with λ light chain. Therefore, the resulting group of 13 'irrelevant' Abs has not been elaborated using a random choice but is composed of Fv crystal structures presenting a significative resemblance with at least one of the 'relevant' structural models. We have preferred to apply a methodology which provides a greater diversity of specificities.

Results and discussion

Construction and presentation of the structural models

Figure 3 summarizes the data related to the construction of 3D models, i.e., the identity (PDB codes) of the selected homologs and their global identity percentages with the studied sequence as well as the position (Kabat numbering) and identity of each SCR or SVRs. For each sequence, we also report the total number of homologs selected after the primary sequence alignments. The values of global identity percentages and the proportion of residues belonging to the SCRs are indicators of the high conservation within the Ig family in terms of primary and secondary structure.

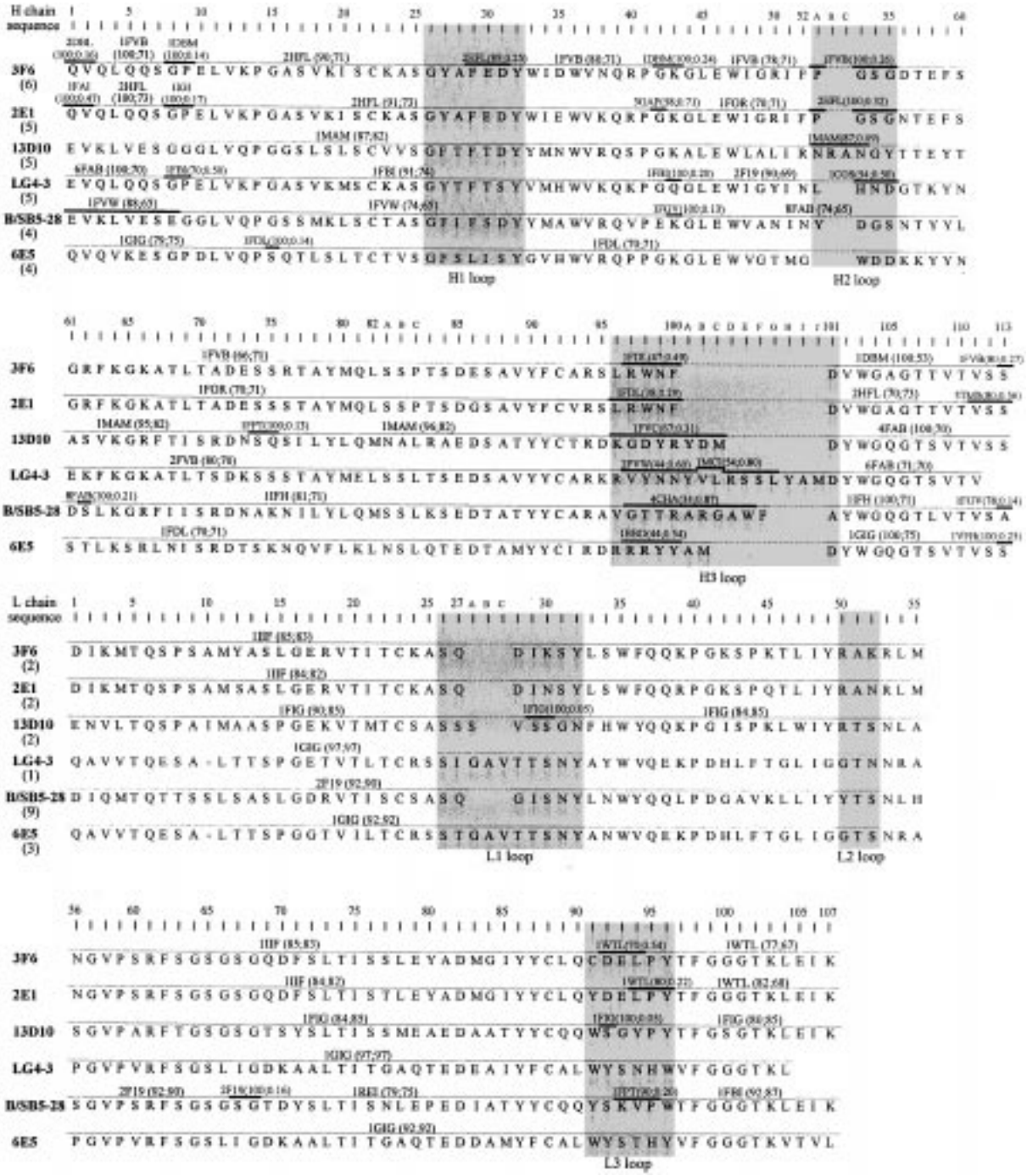

Figure 3. Sequence and main building characteristics of the six anti-(H2A-H2B) mAb variable fragments modeled using the COMPOSER software. For each SCR (thin lines), the PDB code of the homolog used is followed by the percentage of identity calculated for the SCR (first value) and for the whole primary sequence (second value), using the *swiss2* matrix [39]. For SVRs (thick lines), PDB codes, percentages of identity for the fragment and rms distances for the six anchor atoms are indicated. Kabat residue numbering is used. The total number of retained homologs is given in brackets under the name of each Ab. HV loop positions from Chothia and Lesk's work are in gray.

Table 3. PDB codes, identity and characteristics of the mAb of known structure selected either for comparative purposes or as structural templates

PDB code	Ab	Isotype	Resolution (Å)	Specificity	Origin
List of mAbs used for comparative purposes ('irrelevant' mAbs)					
1BBD	8F5	IgG2a κ	2.8	Human rhinovirus serotype 2	Mouse
1DBM	DB3	IgG1 κ	2.7	Progesterone	Mouse
1FBI	F9.13–7	IgG1 κ	3.0	Guinea fowl lysozyme	BALB/c
1FIG	1F7	IgG1 κ	3.0	Catalytic hapten	BALB/c
1FLR	4-4-20	IgG2a κ	1.85	Fluorescein	BALB/c
1FPT	C3	IgG2a κ	3.0	Poliovirus type 1	A/J
1GGB	50.1	IgG2a κ	2.8	HIV-1 (loop 3)	ASW
1GIG	Hc19	IgG1 λ	2.3	Hemagglutinin	Mouse
1IFH	Fab 17/9	IgG2a κ	2.0	Hemagglutinin HA1	BALB/c
1IGI	Fab 26-10	IgG2a κ	2.7	Digoxin	A/J
1MAM	YsT9.1	IgG2b κ	2.45	Surface carbohydrate	Mouse
1RMF	R 6.5	IgG2a κ	2.8	ICAM-1	Mouse
2/3HFL	HyHEL-5	IgG1 κ	2.54	Chicken lysozyme	BALB/c

PDB code	Ab	Model(s), chain	PDB code	Ab	Model(s), chain
Templates used for the construction of model SCRs					
1DBM	DB3	3F6,H	1MAM	YsT9.1	13D10,H
1FBI	F9.13.7	LG4-3,H; B/SB5-28,L	1REI	/REI	B/SB5-28,L
1FDL	D1.3	6E5,H	1WTL	WAT	3F6,L; 2E1,L
1FIG	1F7	13D10,L	2F19	R19.9	LG4-3,H; B/SB5-28,L
1FOR	Fab 17-IA	2E1,H	2FVB	19.1.2	LG4-3,H
1FVB	19.1.2	3F6,H	2HFL	HyHEL-5	3F6,H; 2E1,H
1FVW	W3129	B/SB5-28,H	4FAB	4-4-20	13D10,H
1GIG	Hc19	LG4-3,L; 6E5,H,L	6FAB	36-71	LG4-3,H
1IFH	Fab 17/9	B/SB5-28,H	8FAB	HIL	B/SB5-28,H
1IIF	CB4-1	3F6,L; 2E1,L			
Other templates used for SVRs only					
1BBD	8F5	6E5,H		1MCI	MCG LG4-3,H
1CSG	–	LG4-3,H	1VFB	D1.3	6E5,H
1FAI	Fab R19.9	2E1,H	2DBL	DB3	3F6,H
1FGV	HUH52-AA	B/SB5-28,H	2FVW	W3129	LG4-3,H
1FPT	C3	13D10,H; B/SB5-28,L	3GAP	Not Ig	2E1,H
1FVC	4D5	13D10,H	3TMS	Not Ig	2E1,H
1IGI	Fab 26-10	2E1,H	4CHA	Not Ig	B/SB5-28,H

They could indicate that the knowledge-based method is an appropriate procedure for the construction of Ig fragment 3D structures via comparative molecular modeling.

From Figure 3 it can be seen that the higher the global homology, the shorter the SVRs. In this table we have also reported the position of hypervariable (HV) loops (as defined by Chothia and Lesk [20]). It can be noticed that (i) structural alignments of homolog structures do not systematically lead to SVRs corresponding to HV loops; (ii) these SVRs, when they appear, are shorter than HV regions and (iii) some SVRs are located outside HV regions: other solvent-exposed regions, such as the third framework region (FRW3) of the heavy chains, can also exhibit a structural diversity within the homolog group. These results are consistent with a previous analysis of the possible usefulness of structural databases and sequence alignments [48].

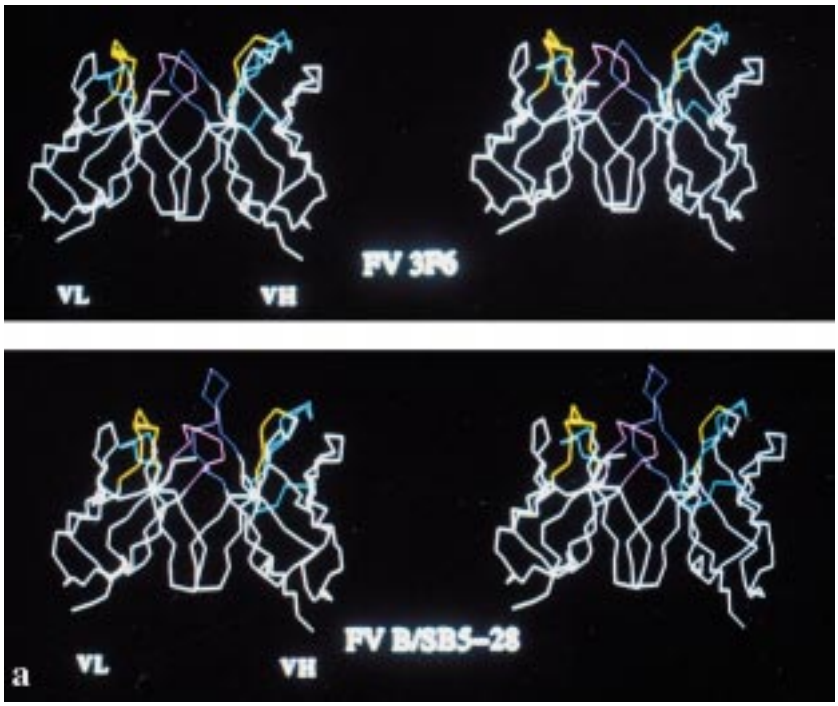

Figure 4. Representative Fv structural models and corresponding Ramachandran diagrams. (a) Stereoscopic C^{α} representations of the modeled Fv fragment of two anti-(H2A-H2B) mAbs: 3F6 and B/SB5-28. The six CDRs are colored with the following code: CDR-1: yellow; CDR-2: green; CDR-H3: violet; CDR-L3: pink. The frameworks are colored in white. (b) Statistical analysis of (φ-ψ) angle distributions (Ramachandran diagram) for the 3F6 and B/SB5-28 Fv models. Heavy (top) and light (bottom) chains have been separated for clarity. Residues in disallowed regions are labeled.

The high conformational variability of the heavy chain third hypervariable region has been previously noted by other authors [49,50] and is responsible for the major uncertainty of the model constructions. Having used the procedure detailed in the Materials and methods section, the criterion for its validation is the measurement and optimization of geometric and stereochemical parameters. It should also be remembered that this particular loop is assumed to be very mobile in solution, more so than other loops, and that its conformation could be affected during the formation of the antibody–antigen complex. Therefore, there is an intrinsic uncertainty of the CDR-H3 conformation which cannot be fully elucidated.

After the energetic minimization of our 3D models, the geometric validation was achieved using the PROCHECK 3.2 software. The most important data of this validation are the Ramachandran diagrams presented in Figure 4 for the VH and VL regions of two representative models: 3F6 and B/SB5-28 (κ and λ light chains, respectively). Satisfactory distributions are observed, and the few residues located outside the favorable areas are always observed at a similar position in the Ramachandran diagram of the corresponding templates. Therefore, it appears that the accuracy of the modeled structures in terms of φ-ψ angle distributions depends to a greater extent on the quality of the experimental structure determination than on the COMPOSER strategy. Furthermore, the influence of the experimental accuracy on the Ramachandran diagram has already been studied [51] and has been shown to play a major role.

Other geometric and structural parameters, such as bond and angle value distributions and exposure of residues to the solvent, were analyzed and were found satisfactory (data not shown).

Analysis of anti-(H2A-H2B) Ab combining sites

Conformational and topographic analysis

It has been suggested that during the formation of an antibody–antigen complex, the contact surface is optimized [49]. Therefore, within a group of Abs of the same specificity, an analysis of the topographic characteristics of their Fv combining sites could provide insights into the binding mechanism. In particular, the

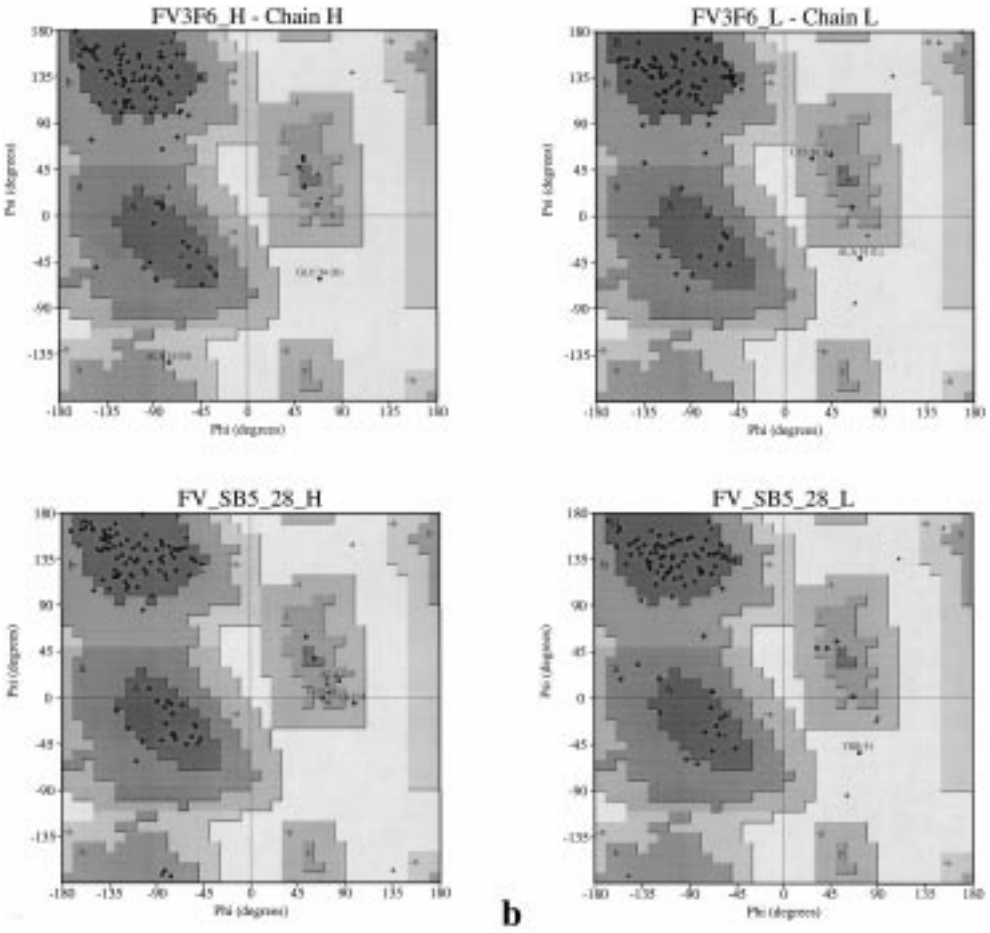

Figure 4. Continued.

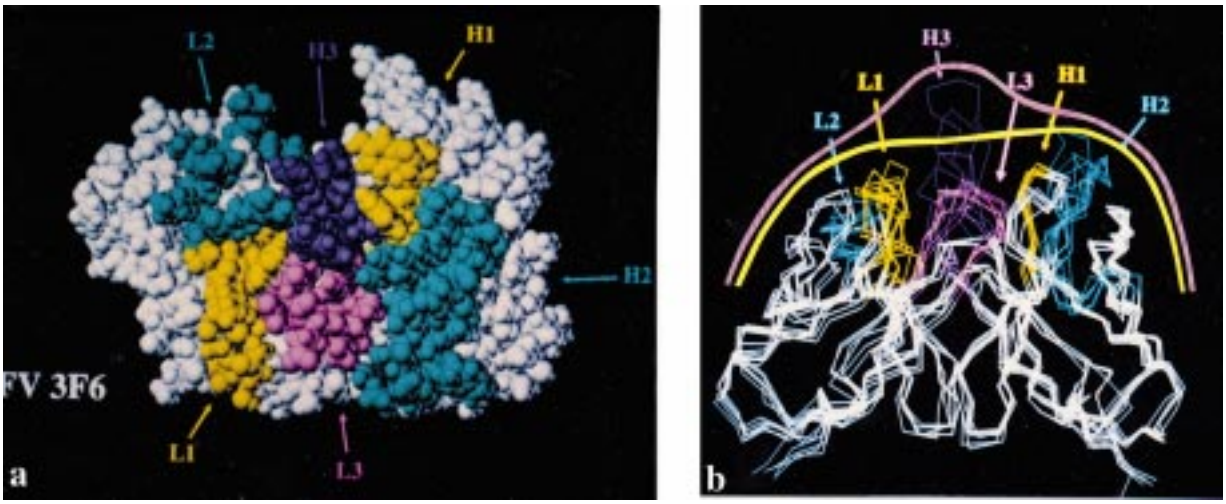

Figure 5. Shape and topography of modeled anti-(H2A-H2B) mAb combining sites. (a) Space-filling representation of the 3F6 Fv structural model. The view is looking directly down into the combining region. The six CDRs are colored according to the same code as in Figure 4a. Similar pictures were used to identify accessible residues during the analysis. (b) C^{α} representation of the structural superimposition of the six anti-(H2A-H2B) mAb Fv models showing the flat or convex topography of the combining sites.

shape of the combining site could be linked to the size of the antigen.

Anti-(H2A-H2B) mAbs exhibit a flat (3F6, 2E1, 13D10, 6E5) or convex (B/SB5-28, LG4-3) geometry of their combining sites (Figure 5), as revealed by space-filling and C^{α} representations of the six Fv antigen-binding sites that allowed their shape to be visualized. The selected Abs of irrelevant activity had, by comparison, clefts or grooves of various depths in certain cases, in particular for Abs which are specific for a small-sized antigen. Hence, it seems that combining sites of Abs adapt their shape and geometry in order to maximize the interaction surface with their antigen. Flat or convex geometries of anti-(H2A-H2B) mAbs are consistent with the large size of these histone dimeric units.

Since some anti-DNA and some anti-nucleosome monoclonal autoAbs have been shown to share genetic and structural characteristics [25], and since filiation relationships might exist between Abs of these two populations, it is of interest to compare the shape and the topographic characteristics of these Abs [52]. According to Eilat and Anderson's [26] work, anti-ssDNA combining sites present a cleft or an incurved cavity on their combining site whereas anti-dsDNA are characterized by a flat topography. Our observation of anti-nucleosome Ab combining sites indicates that they present a shape similar to that of anti-dsDNA Abs. Consequently, if filial relationships exist between anti-DNA and anti-nucleosome autoAbs, they should involve Abs specific to dsDNA rather than ssDNA. Further studies on that subject should also include the understanding of possible relationships between the various populations of anti-DNA Abs (single- and double-stranded DNA).

Electrostatic analysis

We have recently shown [25], from a statistical analysis of primary sequences, that charged residues are overexpressed in anti-nucleosome Ab H-CDRs compared to those of Abs with an irrelevant activity (non-anti-DNA/non-anti-DNA binding proteins). In particular, it was demonstrated that anti-nucleosome Abs include the same high frequency of R residues in their CDR-H3 as do anti-DNA Abs. Nevertheless, these two populations differ by their frequencies of cationic residues: an unusually high percentage of (D+E) residues is observed only for anti-nucleosome Abs in CDR-H1.

Since CDRs, as defined by Kabat et al., do not exactly correspond to the combining site, a 3D approach could lead to a more accurate and detailed analysis of the structure and characteristics of these combining sites. Therefore, physicochemical properties of the combining sites that depend on the nature of the accessible amino acids, on the loop conformations and on the relative location of residue side chains can be investigated.

One way to establish the presumed role of ionic interactions in the binding of anti-nucleosome Abs to their cognate antigen is to compute the electrostatic potentials on Fv molecular surfaces. Figure 6 presents the electrostatic patterns obtained with the MOLCAD software for the six anti-(H2A-H2B) Ab Fv models. The simultaneous observation of the six electrostatic profiles does not allow an easily recognizable common electrostatic pattern to be identified among the anti-(H2A-H2B) mAbs. However, two subgroups can be defined on the basis of major electrostatic quantitative differences. The first one (group I: 3F6, 2E1 and 13D10 Abs) is characterized by a strong dominance of negative zones, by contrast with the second one (group II: LG4-3, B/SB5-28 and 6E5 Abs) which is characterized by a combining site surface dominated by neutral potentials and positive areas.

More precisely, in group I, electrostatic potentials are organized as large negative areas covering about 70% of combining site accessible residues, inequally distributed on both VH and VL surfaces. For 3F6 and 2E1 Abs, the negative surface lies on four of the six CDRs, namely CDR-L1, -L3, -H1 and -H2. For 13D10, the more intense negative area covers the two CDR-3 and tends to spread over the CDR-L1. On the 3F6 Ab MOLCAD picture, a limited highly positive surface can be seen at the interface between CDR-H3 and -L2. The absence of such a zone on the 2E1 model is the main difference between this Ab and 3F6. 13D10 exhibits a similar but smaller and weaker positive zone.

In group II, no negative area can be distinguished with the exception of a small area covering part of the B/SB5-28 CDR-H2. In contrast, positive area localized in the vicinity (6E5) or at the center (LG4-3 and B/SB5-28) of the combining site characterizes the Abs of this group. These electrostatic features are similar to those of the two anti-ssDNA mAbs (4B1 [53] and BV04-01 [54]) for which electrostatic surface representation (Figure 7) showed a positive central zone slightly more extensive than the one observed for LG4-3 and B/SB5-28. Previous studies devoted to directed mutagenesis experiments [55] and structural determination of anti-DNA Abs [54,56–58]

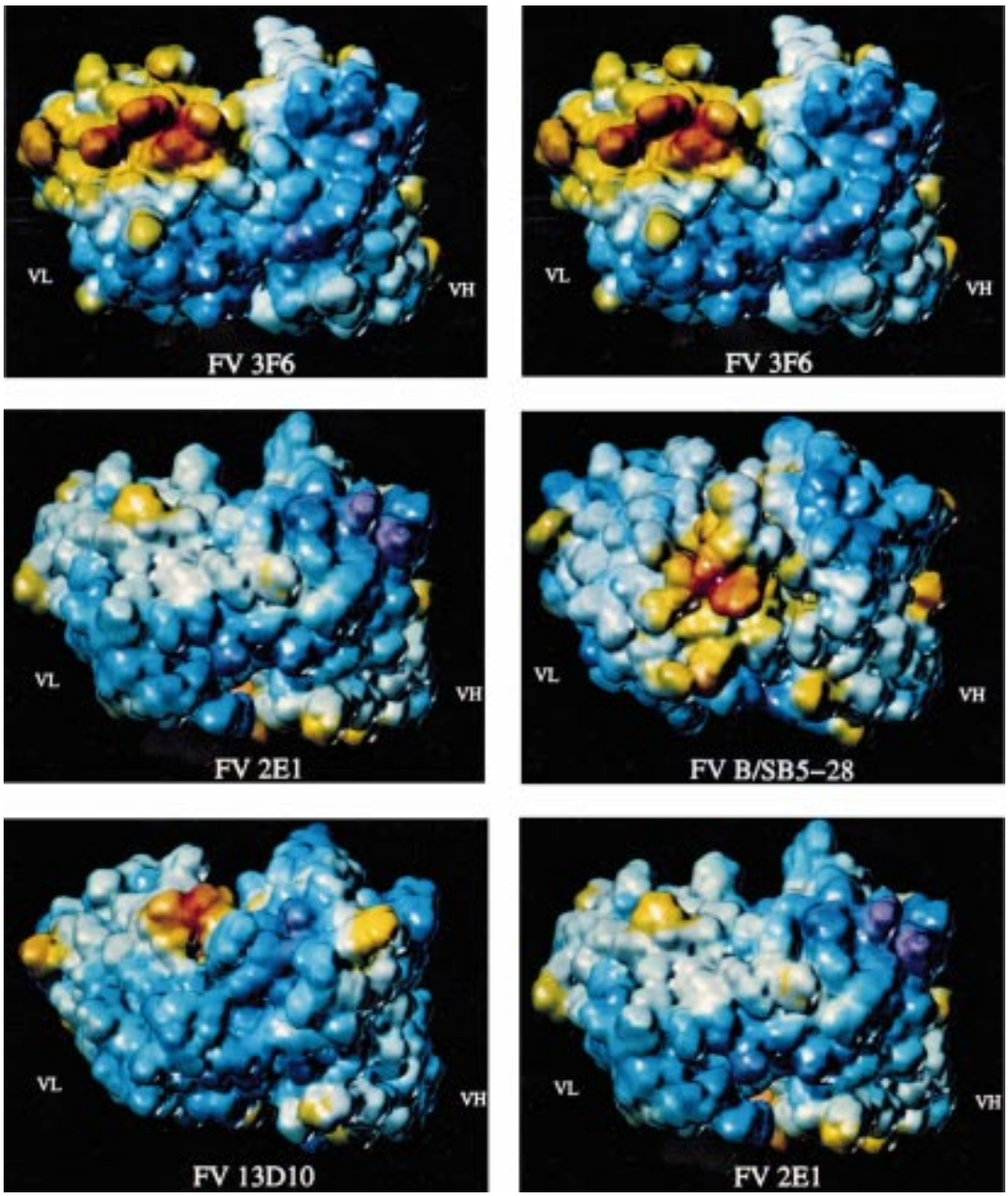

Figure 6. Electrostatic potentials of the six anti-(H2A-H2B) mAb combining site surfaces. Molecular surfaces and electrostatic patterns were computed using the MOLCAD software. The most negative zones are blue-colored and the most positive ones are in red. The orientation is that of Figure 5a.

have established the major role of basic (mainly arginine) residues in the recognition of DNA by autoAbs. Further evidence in support of this hypothesis was provided by the computation of electrostatic potentials on anti-ssDNA and anti-dsDNA Ab combining sites. This computation revealed the presence of dominating positive regions [57–59]. Hence, our results are consistent with the DNA binding activity demonstrated for two (LG4-3 and 6E5) out of the three group II members, whereas none of the group I members have such an activity.

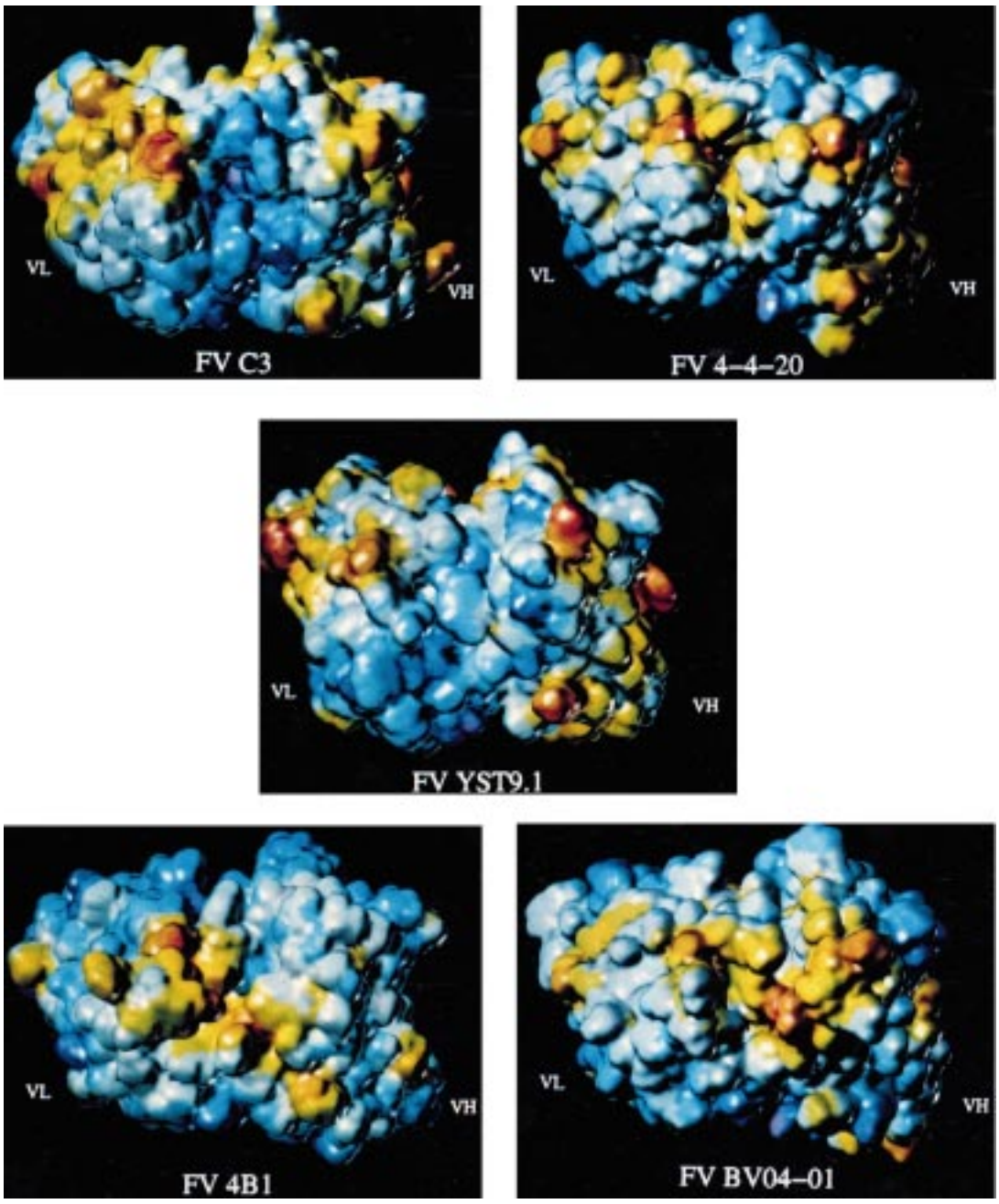

Figure 7. Electrostatic potentials of irrelevant (top two rows; C3, 4-4-20 and YsT9.1) and anti-ssDNA (bottom row; 4B1 and BV04-01) mAb combining sites. Orientation and color codes are the same as for Figure 6.

For comparative purposes, we have also calculated the electrostatic potentials on Fv surfaces of the 13 irrelevant Abs listed in Table 3. Figure 7 presents the combining site electrostatic potential for three of these irrelevant Abs chosen as representative of the whole irrelevant mAb group. Like the vast majority of the members of this group, C3 [60], 4-4-20 [61] and YsT9.1 [62] exhibit charged surface potentials and different patterns. C3 is a prototype of the Abs with a negative central region, 4-4-20 represents the positive central region Abs, and YsT9.1 has been chosen for its alternating of small positive and negative areas.

The comparison between Fv C3, which exhibits the most negative surface, and group I members indicates that the negative potential of the latter is clearly more extensive and intense than that of the irrelevants. Moreover, the more strongly negative residues of the C3 Ab combining site are located at the inner side of a well and therefore are hardly accessible. Although little resemblance between YsT9.1 and relevant Abs can be noticed, it is of interest to highlight that 4-4-20 Ab exhibits an electrostatic pattern quite similar to those of group II members and of anti-ssDNA mAbs.

Hence, the analysis of combining site electrostatic potentials reveals that our selected anti-(H2A-H2B) mAbs form a heterogeneous population without correlation with the genetic origin of the mAbs. Two subgroups of distinct electrostatic patterns have been established and suggest different probable binding mechanisms of the (H2A-H2B) dimer. The first subgroup members are likely to recognize the (H2A-H2B) dimer via electrostatic attraction and possible formation of ionic bonds since their surface potentials are strongly negative, differing from those of all the irrelevant and anti-ssDNA Abs. Such a mechanism corresponds to our main hypothesis. Nevertheless, this hypothesis does not hold for the second subgroup members of anti-(H2A-H2B) Abs which do not show large negative areas and which furthermore present similarities with anti-DNA Abs and some of the irrelevant Abs.

Therefore, this evident electrostatic diversity suggests that the specificity against the (H2A-H2B) dimer cannot be attributed in all cases to a significant and conserved negative potential on the combining site surfaces. It must be assumed that electrostatic surface representations are not sufficient by themselves to identify a common strongly prevailing recognition mechanism of histones based on electrostatic complementarity.

The lack of a unique electrostatic pattern for anti-histone Abs led us to envisage two explanations: (i) the binding process could be based on ionic interactions that are so subtle or confined that they cannot be easily observed; and (ii) the binding process is not ubiquitously governed by ionic interactions and multiple anti-histone recognition mechanisms should be considered.

This global analysis of possible ionic interactions with an antigen has been completed by determining the accessible charged residues, in order to explain the electrostatic potentials observed in terms of the quantity, location and nature of these charged residues. In Table 4, we present the number of accessible anionic (D, E) and cationic (R, K) residues throughout the combining site of the three previously represented Ab populations (anti-(H2A-H2B), irrelevant and anti-DNA Abs). Among the accessible residues, those of the framework located in the vicinity of the CDRs (Kabat definition) were also taken into account. This counting of charged residues also allowed the identification of intramolecular ionic bonds resulting from the presence of closely located residues of opposite charges. These residues are therefore available for an interaction with an antigen but only through a competitive process.

As suggested by sequence analyses [25], Table 4 analysis shows that anti-(H2A-H2B) and anti-DNA Abs contain a significantly greater quantity of accessible charged residues. Among anti-(H2A-H2B) Abs, the two subgroups defined by surface electrostatic potential analysis are recovered, since the three Abs belonging to group I (3F6, 2E1 and 13D10) present the larger amount of acidic residues, which can explain their negative dominance. However, for 3F6 and 13D10 mAbs, the presence of very similar quantities of acidic and basic residues results in negative areas and quite limited positive zones. This striking feature can be partly explained by a cumulative effect of closely positioned acidic residues whereas basic ones are more often isolated. Moreover, the large size of basic residue side chains means the positive charge is distributed over a greater volume. By contrast, the negative charge is concentrated on the carboxylic group in acidic residues.

For the second subgroup, the analysis of charged residue positions is consistent with the electrostatic patterns obtained. The absence or the weak representation of negative areas can be mainly explained by the lack of glutamic acid residues, referred to members of the first subgroup. In fact, the major particularity of group I is an unusual quantity of accessible E residues compared with irrelevant and anti-DNA Abs. Among the exposed cationic residues, arginine is also significantly overrepresented in the anti-(H2A-H2B) Abs; this feature can also be observed for anti-DNA Abs and has already been demonstrated, from primary sequence analyses, to be a characteristic of anti-dsDNA Abs [63].

In order to explain the lack of significant negative areas on the combining sites of group II anti-(H2A-H2B) Abs, we have envisaged that antigen–antibody complex formation could involve cation-π interactions [28]. Since histones are known to present cationic

Table 4. Count of selected amino acids accessible on the Ab combining site surfaces of anti-(H2A-H2B), irrelevant and anti-ssDNA mAbs[a]

	Ionic interactions					Cation-π interactions			
	D	E	R	K	Σ	F	Y	W	Σ
3F6	5	4	4	3	16	2	4	2	8
2E1	4	4	3	1	12	3	3	2	8
13D10	3	2	4	1	10	0	6	1	7
LG4-3	2	1	3	3	9	0	7	0	7
B/SB5-28	4	0	2	2	8	0	8	1	9
6E5	3	0	3	3	9	0	7	1	8
Mean	3.5	1.8	3.2	2.2	10.7	0.8	5.8	1.2	7.8
Irrelevant Abs									
Mean	2.7	0.7	1.5	1.9	6.8	0.4	5.3	1.0	6.7
Anti-DNA Abs									
Mean	2.5	0.5	3.5	2.5	9.0	0.5	4.0	1.5	6.1

[a] Amino acids are grouped according to their possible interaction types. Mean values are given for charged residues of the three populations. The last column (Σ) of each group is the sum of the residues considered.

terminal chains, we have identified and counted, on antigen binding sites, the accessible aromatic residues. The obtained values, summarized in Table 4, indicate that no important differences exist between anti-(H2A-H2B) and irrelevant Abs. Nevertheless, Y residues are overexpressed for group II members and could therefore be responsible for a potentiality of cation-π interactions. Such interactions could at least partially compensate for the weaker potentiality of classical ionic interactions.

Towards the understanding of Ab properties and behaviors

Binding mechanism of anti-(H2A-H2B) Abs

From our models and the electrostatic patterns calculated on their combining site surfaces, a unique recognition mechanism of the nucleosome cannot be proposed. Therefore, it is likely that two distinct binding mechanisms of anti-(H2A-H2B) Abs to their antigen should be envisaged (Figure 8) in connection with the existence of the two groups defined above on the basis of electrostatic patterns. On the one hand, group I members, characterized by a strong negative potential, could interact with the positive parts of histones (in particular the N- and C-terminal regions) mainly through ionic bonds. On the other hand, group II members, which do not present a significant negative potential on their combining site, could bind the antigen through another mechanism involving neutral residues forming a conformational epitope.

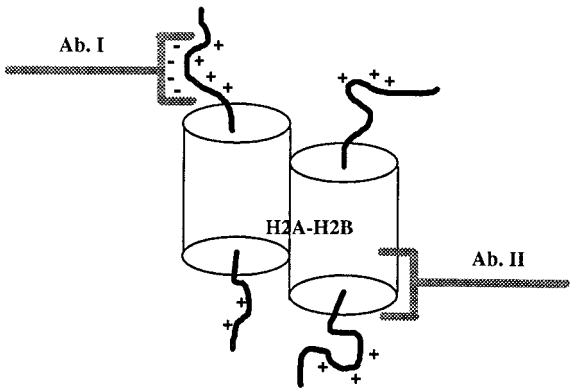

Figure 8. Hypothetical interaction mechanisms for the two groups of anti-(H2A-H2B) mAbs. The Abs of group I (Ab-I) are likely to interact with the (H2A-H2B) dimer through an ionic binding mechanism involving anionic residues of the Ab combining site and cationic amino acids of the histone terminal domains. The Abs of group II (Ab-II) are assumed to interact with the dimer through the recognition of a conformational epitope.

Consequences for further experimental studies

These hypotheses suggested by the analysis of the 3D models can be considered as a first step in the development of our continuing research program. More precisely, new experiments could be elaborated in order to test the above speculative hypotheses. Preliminary results have already shown that the binding of group I members is decreased when the NaCl concentration is increased in the medium (data not shown). This evidence supports the ionic interaction model between these Abs and the histones. The variation of ionic

binding capabilities between the two groups is currently under investigation with different biochemical techniques.

Site-directed mutagenesis will also be used to determine the influence of specific residues. In particular, the replacement of anionic residues by neutral or basic residues may confirm whether or not ionic bonds form and, if so, where they form. Using the same technique, the replacement of complete CDRs or HV loops would allow a study of the importance of the flexibility of these loops and therefore an evaluation of the conformational constraints.

The involvement of histone terminal regions could be tested by looking for variations in the activity of various antigens upon deletion of the terminal regions by enzymatic digestion.

Relationships between anti-(H2A-H2B) and anti-DNA Abs

Kinetic studies using lupus murine models have established that anti-nucleosome Abs appear before anti-DNA Abs [64,65]. Furthermore, our previous works have shown that anti-nucleosome and anti-DNA mAbs present common structural features [25]. Assuming that filial relationships could exist between the two populations, our analysis of electrostatic patterns indicates that these relationships could be restricted to one subpopulation, namely group II members, since they have been shown to present similar electrostatic properties to anti-DNA Abs. Therefore, our results lead us to suggest that mAbs of group II could be responsible for the subsequent appearance of anti-DNA Abs, constituting a source of anti-dsDNA Abs.

Influence on pathogenic properties

Significant quantities of both anti-DNA and anti-nucleosome Abs are present in SLE patients' sera [66]. Numerous studies devoted to anti-DNA Abs have revealed the pathogenic role of certain Ab subpopulations, although the characteristics of these pathogenic Abs remain enigmatic [53]. The possible relationships between anti-DNA and anti-nucleosome Abs lead us to envisage the possible pathogenic character of anti-nucleosome Abs. Furthermore, some drugs are known to induce a lupic syndrome characterized by the presence of anti-nucleosome Abs and the absence of anti-DNA Abs [23]. These observations suggest that anti-nucleosome Abs play an important role in pathogenesis, and our hypothesis that two groups of anti-nucleosome Abs can be distinguished on the basis of their electrostatic pattern leads us to consider a possible link between electrostatic pattern and pathogenicity. The pathogenic properties of group I and group II anti-(H2A-H2B) Abs are under investigation, by means of direct injection of hybridomas in mouse [53].

Conclusions

Our study shows that a knowledge-based molecular modeling approach can lead to important insights into structure–function and structure–origin relationships of Abs. For anti-(H2A-H2B) mAbs, the analyses of combining site surface properties revealed a topographic homogeneity. However, a unique antibody–antigen interaction mechanism based on predominating ionic interactions is not supported, suggesting that anti-(H2A-H2B) mAbs constitute a heterogeneous population. Interestingly, our results indicate that one subpopulation does resemble anti-DNA mAbs. Several of our observations support the hypothesis of the nucleosome as a major antigen eliciting both anti-DNA and anti-(H2A-H2B) autoAbs during the course of systemic lupus erythematosus.

Hence, the present molecular modeling study reinforces some of our previous results and leads us to formulate several hypotheses about the origin of anti-(H2A-H2B) Abs and their binding mechanism at a molecular level. Thus, in addition to its general interest, molecular modeling is a useful tool allowing more rapid and accurate experimental developments and investigations. Despite these major contributions, care should be exercised when considering data generated from a knowledge-based modeling study. Such theoretical approaches should always be followed by systematic experiments which test the hypotheses derived from the models.

Acknowledgements

We wish to thank Sophie Koutouzov for giving us her immunoglobulin sequence data, Carolyn Cho and Jeff Stewart for valuable discussions and for correcting the manuscript. This work was supported by a grant from the Institut National de la Santé et de la Recherche Médicale (INSERM CRI 950602 to F.T.). F.B. is a postdoctoral fellow supported by the 'Fondation pour la Recherche Médicale' and 'La Région de Haute-Normandie'.

References

1. Bryson, J.W., Betz, S.F., Lu, H.S., Suich, D.J., Zhou, H.X., O'Neil, K.T. and DeGrado, W.F., Science, 270 (1995) 935.

2. Janin, J., Proteins, 21 (1995) 30.
3. Janin, J., Biochimie, 77 (1995) 497.
4. McPherson, A., The Preparation and Analysis of Protein Crystal, Wiley, New York, NY, 1982.
5. Zhao, D. and Jardetzky, O., J. Mol. Biol., 239 (1994) 601.
6. Overington, J.P., Curr. Opin. Struct. Biol., 2 (1992) 394.
7. Böhm, G., Biophys. Chem., 59 (1996) 1.
8. Sanchez, R. and Sali, A., Curr. Opin. Struct. Biol., 7 (1997) 206.
9. Hilbert, M., Böhm, G. and Jaenicke, R., Proteins, 17 (1993) 138.
10. Bruccoleri, R.E., Mol. Simul., 10 (1993) 151.
11. Tenette, C., Ducancel, F. and Smith, J.C., Proteins, 26 (1996) 9.
12. Martin, A.C.R., Cheetham, J.C. and Rees, A.R., Proc. Natl. Acad. Sci. USA, 86 (1989) 9268.
13. Alzari, P.M., Lascombe, M.B. and Poljak, R.J., Annu. Rev. Immunol., 6 (1988) 555.
14. Viswanathan, M., Anchin, J.M., Droupadi, P.R., Mandal, C., Linthicum, D.S. and Subramaniam, S., Biophys. J., 69 (1995) 741.
15. Tramontano, A. and Lesk, A.M., Proteins, 13 (1992) 231.
16. Wilson, I.A. and Stanfield, R.L., Curr. Opin. Struct. Biol., 3 (1993) 113.
17. Mian, I.S., Bradwell, A.R. and Olson, A.J., J. Mol. Biol., 217 (1991) 133.
18. Kabat, E.A., Wu, T.T., Perry, H.M., Gottesman, K.S. and Foeller, C., Sequences of Proteins of Immunological Interest, U.S. Government Printing Office, National Institutes of Health, Bethesda, MD, 1991.
19. Chothia, C. and Lesk, A.M., J. Mol. Biol., 196 (1987) 901.
20. Chothia, C., Lesk, A.M., Tramontano, A., Levitt, M., Smith-Gill, S.J., Air, G., Sheriff, S., Padlan, E.A., Davies, D., Tulip, W.R., Colman, P.M., Spinelli, S., Alzari, P.M. and Poljak, R.J., Nature, 342 (1989) 877.
21. Kotzin, B.L., Cell, 85 (1996) 303.
22. Arents, G., Burlingame, R.W., Wang, B., Love, W.E. and Moudrianakis, E.N., Proc. Natl. Acad. Sci. USA, 88 (1991) 10148.
23. Monestier, M. and Kotzin, B.L., Rheum. Dis. Clin. North Am., 18 (1992) 415.
24. Theofilopoulos, A.N. and Dixon, F.J., Adv. Immunol., 37 (1985) 269.
25. Brard, F., Jovelin, F., Petit, S., Tron, F. and Gilbert, D., Eur. J. Immunol., 26 (1996) 1587.
26. Eilat, D. and Anderson, W.F., Mol. Immunol., 31 (1994) 1377.
27. Radic, M.Z. and Weigert, M., Annu. Rev. Immunol., 12 (1994) 487.
28. Dougherty, D.A., Science, 271 (1996) 163.
29. Portanova, J.P., Creadon, G., Zhang, X., Smith, D.S., Kotzin, B.L. and Wysocki, L.J., Mol. Immunol., 32 (1995) 117.
30. Losman, M.J., Fasy, T.M., Novick, K.E. and Monestier, M., Int. Immunol., 5 (1993) 513.
31. Vasquez, M., Némethy, G. and Scheraga, H.A., Chem. Rev., 94 (1994) 2183.
32. Sali, A., Overington, J., Johnson, M.S. and Blundell, T.L., Trends Biol. Sci., 15 (1990) 235.
33. Srinivasan, N. and Blundell, T.L., Protein Eng., 6 (1993) 501.
34. SYBYL, Molecular Modeling Software v. 6.2, Theory Manual, Tripos Associates, St. Louis, MO, 1995.
35. Sali, A. and Blundell, T.L., J. Mol. Biol., 212(1990) 403.
36. Overington, J., Johnson, M.S., Sali, A. and Blundell, T.L., Proc. R. Soc. London, B241 (1990) 132.
37. Bernstein, F.C., Koetzle, T.F., Williams, G.J., Meyer Jr., E.E., Brice, M.D., Rodgers, J.R., Kennard, O., Shimanouchi, T. and Tasumi, M., J. Mol. Biol., 112 (1977) 535.
38. Needleman, S. and Wunsch, C., J. Mol. Biol., 48 (1970) 443.
39. Gonnet, G.H., Cohen, M.A. and Benner, S.A., Science, 256 (1992) 1443.
40. Powell, M.J.D., Math. Program., 12 (1977) 241.
41. Weiner, S.J., Kollman, P.A., Case, D.A., Singh, U.C., Ghio, C., Alagona, G., Profeta, S. and Weiner, P.K., J. Am. Chem. Soc., 106 (1984) 765.
42. Weiner, S.J., Kollman, P.A., Nguyen, D.T. and Case, D.A., J. Comput. Chem., 7 (1986) 230.
43. Singh, U.C. and Kollman, P.A., J. Comput. Chem., 5 (1984) 129.
44. Laskowski, R.A., MacArthur, M.W., Moss, D.S. and Thornton, J.M., J. Appl. Crystallogr., 26 (1993) 283.
45. Martin, A.C.R., Proteins, 25 (1996) 130.
46. Heiden, W., Goetze, T. and Brickmann, J., J. Comput. Chem., 14 (1993) 246.
47. Connolly, M.L., J. Appl. Crystallogr., 16 (1983) 548 (QCPE Program No. 429, 'Molecular Surface Program').
48. Sander, C. and Schneider, R., Proteins, 9 (1991) 56.
49. Padlan, E.A., Mol. Immunol., 31 (1994) 169.
50. Wu, T.T., Johnson, G. and Kabat, E.A., Proteins, 16 (1993) 1.
51. Johnson, M.S., Srinivasan, N., Sowdhamini, R. and Blundell, T.L., Crit. Rev. Biochem. Mol. Biol., 29 (1994) 1.
52. Brard, F., Gilbert, D., Jovelin, F. and Tron, F., J. Autoimmun. (1997) in press.
53. Gilbert, D., Brard, F., Margaritte, C., Delpech, A. and Tron, F., Mol. Immunol., 32 (1995) 477.
54. Herron, J.N., He, X.M., Ballard, D.W., Blier, P.R., Pace, P.E., Bothwell, A.L.M., Voss Jr., E.W. and Edmundson, A.B., Proteins, 11 (1991) 159.
55. Radic, M.Z., Mackle, J., Erikson, J., Mol, C., Anderson, W.F. and Weigert, M., J. Immunol., 150 (1993) 4966.
56. Cygler, M., Boodhoo, A., Lee, J.S. and Anderson, W.F., J. Biol. Chem., 262 (1987) 643.
57. Mol, C.D., Muir, A.K.S., Lee, J.S. and Anderson, W.F., J. Biol. Chem., 269 (1994) 3605.
58. Mol, C.D., Muir, A.K.S., Cygler, M., Lee, J.S. and Anderson, W.F., J. Biol. Chem., 269 (1994) 3615.
59. Barry, M.M., Mol, C.D., Anderson, W.F. and Lee, J.S., J. Biol. Chem., 269 (1994) 3623.
60. Wien, M.W., Filman, D.J., Stura, E.A., Guillot, S., Delpeyroux, F., Crainic, R. and Hogle, J.M., Nat. Struct. Biol., 2 (1995) 232.
61. Herron, J.N., Terry, A.H., Johnston, S., He, X.M., Guddat, L.W., Voss, E.W. and Edmundson, A.B., Biophys. J., 67 (1994) 2167.
62. Rose, D.R., Przybylska, M., To, R.J., Kayden, C.S., Oomen, R.P., Vorberg, E., Young, N.M. and Bundle, D.R., Protein Sci., 2 (1993) 1106.
63. Shlomchik, M.J., Mascelli, M.A., Shan, H., Radic, M.Z., Pisetsky, D.S., Marshak-Rothstein, A. and Weigert, M., J. Exp. Med., 171 (1990) 265.
64. Amoura, Z., Chabre, H., Koutouzov, S., Lotton, C., Cabrespines, A., Bach, J.F. and Jacob, L., Arthritis Rheum., 37 (1994) 1684.
65. Burlingame, R.W., Rubin, R.L., Balderas, R.S. and Theofilopoulos, A.N., J. Clin. Invest., 91 (1993) 1687.
66. Chabre, H., Amoura, Z., Piette, J.C., Godeau, P., Bach, J.F. and Koutouzov, S., Arthritis Rheum., 38 (1995) 1485.